POLITECNICO DI TORINO
Repository ISTITUZIONALE

Advanced Feature Analysis of Eddy Current Testing Signals for Rail Surface Defect Characterization

Original
Advanced Feature Analysis of Eddy Current Testing Signals for Rail Surface Defect Characterization / Quercio, M., Santoro, L., Sesana, R., Riganti Fulginei, F.. - In: IEEE ACCESS. - ISSN 2169-3536. - 13:(2025), pp. 1-15. [10.1109/ACCESS.2025.3597079]

Availability:
This version is available at: 11583/3002376 since: 2025-08-09T09:19:28Z

Publisher:
IEEE

Published
DOI:10.1109/ACCESS.2025.3597079

Terms of use:

This article is made available under terms and conditions as specified in the corresponding bibliographic description in the repository

Publisher copyright

(Article begins on next page)

19 November 2026

IEEE Access
Multidisciplinary | Rapid Review | Open Access Journal

Received 14 July 2025, accepted 6 August 2025, date of publication 8 August 2025, date of current version 15 August 2025.

Digital Object Identifier 10.1109/ACCESS.2025.3597079

RESEARCH ARTICLE

Advanced Feature Analysis of Eddy Current Testing Signals for Rail Surface Defect Characterization

MICHELE QUERCIO[1], LUCA SANTORO[2], RAFFAELLA SESANA[2], AND FRANCESCO RIGANTI FULGINEI[1], (Member, IEEE)

[1]Department of Industrial, Electronic and Mechanical Engineering, Roma Tre University, 00146 Rome, Italy
[2]Department of Mechanical and Aerospace Engineering, Politecnico di Torino, 10129 Turin, Italy

Corresponding author: Michele Quercio (michele.quercio@uniroma3.it)

ABSTRACT The maintenance of the railways is of paramount importance for safe and reliable transport. Eddy Current Testing (ECT) provides high-resolution time-series signals that capture subtle anomalies on the rail surface. This paper expands on previous analyses by combining classical time-frequency methods (short-time Fourier transform and continuous wavelet transform) and estimation of fractal dimensions with *advanced feature extraction* approaches, including wavelet sub-band decomposition, Hilbert–Huang transform, peak analysis and entropy metrics. Subsequently, a Random Forest classifier is applied to each set of characteristics, and we report comparative accuracy results on a dataset comprising rail segments with *joints*, *welds*, or *squats*. Experimental findings reveal that the Hilbert–Huang transform features yield the highest accuracy (93.28 %), while simpler features, such as peak counts, are less discriminative (46.93 %). These results underscore the effectiveness of using multiple signal-decomposition strategies and advanced analytics to robustly detect and categorize surface defects for better rail-maintenance decisions.

INDEX TERMS Continuous wavelet transform, eddy current testing, fractal dimension, Hilbert-Huang, peak analysis, rail surface defects, STFT, wavelet subbands.

I. INTRODUCTION

The reliability and safety of railway infrastructure depend largely on the timely detection and characterization of surface or subsurface defects in rails. In the realm of heavy-haul and high-speed operations, such defects can cause premature wear, Rolling Contact Fatigue (RCF), cracks, and even catastrophic rail failures if left unmonitored [1], [2], [3], [4], [5]. In particular, RCF can initiate microscopic crack networks on the rail head, which then propagate and threaten train stability, thus motivating intensive research efforts into nondestructive inspection techniques and robust defect classification schemes. Advanced nondestructive testing (NDT) methods have emerged for different applications and in particular for railway inspection, aiming to balance cost-effectiveness with stringent accuracy requirements [6], [7], [8], [9], [10].

The associate editor coordinating the review of this manuscript and approving it for publication was Jesus Felez.

Beyond conventional visual checks, eddy current testing (ECT) and other electromagnetic-based approaches allow for in-service identification of near-surface cracks, while ultrasonic or magnetic flux leakage (MFL) methods can penetrate deeper into the rail. Recent studies emphasize the efficiency gains of real-time defect detection during scheduled runs or specialized inspection trains. Complexities arise in developing sensors and scanning schemes capable of high-speed data acquisition on fast-moving vehicles without sacrificing resolution [11], [12], [13], [14], [15]. Indeed, lifts or geometric irregularities of probes can degrade signal clarity, demanding robust calibration and advanced signal processing. The proliferation of massive data sets generated by dense sensor arrays also calls for advanced algorithms to effectively interpret electromagnetic signatures and translate them into actionable defect characterizations. Within modern railway maintenance planning, the impetus to reduce total life-cycle costs is significant [16]. On one side,

© 2025 The Authors. This work is licensed under a Creative Commons Attribution 4.0 License.
For more information, see https://creativecommons.org/licenses/by/4.0/

underestimating defect severity can increase derailment risk, whereas overestimation leads to unnecessary rail grinding and part replacements. Consequently, machine learning and data-fusion-based techniques are increasingly proposed to classify defect types (e.g. squats, head checks, weld transitions) and estimate their depth or growth rate. Such classification aids in formulating more strategic maintenance scheduling, from small spot repairs to larger track renewal programs. Studies on the correlation between electromagnetic signals and actual mechanical crack dimensions are abundant, especially for surface microcracks and near-surface RCF [17], [18], [19]. These contributions often highlight advanced sensor architectures, such as multi-coil arrays or rosette-type eddy current probes, improving detection performance for angled defects. Some approaches further incorporate multi-frequency or pulsed-thermography analyses, extracting time-frequency patterns that reveal microstructural discontinuities. Despite the advantages of electromagnetic methods, key challenges remain. For instance, abrupt weld transitions or wheel burns on the rail surface can mask certain defect signatures [20], [21], [22]. Similarly, environmental interference and variation in rail steel grades require sensor calibration for consistent data acquisition. The analysis of raw signals is often coupled with structural models of wheel–rail interactions, thereby helping to isolate defect-specific waveforms from generic mechanical noise. Improvement in raw signal detection is closely intertwined with transducer geometry. Some works explore specialized magnetic pole configurations or novel Halbach arrays to maximize the signal-to-noise ratio in eddy current data [23], [24], [25]. Others delve into 3D finite element analysis to simulate coil–rail interactions, elucidating how sensor placement and coil orientation affect detection depth and surface coverage. Recent decades have seen an expanded use of synergy between mechanical models and advanced sensor hardware for integrated structural health monitoring (SHM) in railway lines [26], [27], [28]. Solutions combining eddy current signals with temperature profiles, acoustic emission data, or real-time vibration measurements can provide robust multi-physics coverage of rail integrity. By correlating signals from diverse sensing modalities, one can resolve ambiguities that might arise from an isolated technique. Onboard computing improvements have also driven attention to data fusion at the train level [29], [30]. This can include merging wheel–rail friction conditions and historical track defect records to guide the classifier in assigning likely flaw categories. Intelligent software platforms, sometimes integrated with geographic information systems, can visualize defect distributions, enabling track managers to prioritize maintenance with spatial awareness. Integrating advanced wavelet-based or fractal dimension-based analytics has yielded encouraging results for differentiating genuine cracks from superficial damage [31], [32]. For instance, fractal dimension can capture subtle signal fluctuations reflective of microcrack complexity. In parallel, wavelet subband features can reveal multi-scale temporal–spectral structures of eddy current waveforms. Meanwhile, Hilbert–Huang Transform (HHT) adds an adaptive decomposition perspective, enabling detection of modulated crack signals under non-stationary conditions. Turnouts, weld zones, and insulated joints likewise pose detection complexity: the abrupt changes in local geometry or material composition can generate spurious signals. While some literature underscores the promise of wavelet or fractal-based feature extraction for classification, others exploit advanced machine learning strategies, such as neural networks or support vector machines, to recognize patterns in the amplitude–phase domain [33], [34], [35], [36]. Under field conditions, these algorithms must handle environmental noise and mechanical disturbances, placing a premium on robust training data sets that reflect diverse usage scenarios. Investigations into the synergy of mechanical and microstructural changes show that eddy current signals can be correlated with different crack propagation stages [37]. This in turn fosters early repair strategies that mitigate further crack growth, potentially halving maintenance costs. Complementary fractographic analyses can validate NDT findings, helping calibrate classification thresholds by referencing destructive tests. Still, novel structural concepts and design improvements—such as new composite materials for certain rail components or specialized damping strategies—continue to emerge [38], [39]. Multi-physics modeling ties in the ECT coil geometry, steel electromagnetic parameters, and mechanical dynamic loads from passing trains. Summarily, this fosters a powerful environment for sensor design iteration before expensive track testing. Against this backdrop, the present study proposes an *extended analysis pipeline* for ECT signals, merging classical time-frequency transforms (STFT, CWT) with fractal dimension analysis and advanced feature extraction. The core contribution of this paper is to systematically compare the classification performance of different feature extraction methods, including wavelet subband decomposition, Hilbert-Huang transform, peak analysis, and entropy metrics, in quantifying rail defect signatures. We aim to systematically compare various features in quantifying rail defect signatures, including near-surface cracks and more complex damage modes. The objective of this research are:

1) Establish an end-to-end analytical pipeline that unifies classical time–frequency tools, fractal geometry and four advanced feature families for ECT signals.
2) *Systematically compare* the classification performance, computational burden and real-time suitability of those feature families on the same benchmark dataset.
3) Quantify the influence of nuisance factors (environmental noise, class imbalance) and outline the method's portability to other nondestructive-testing sensors.

While Eddy Current Testing (ECT) has been widely used for rail surface defect detection due to its high sensitivity and resolution, the effectiveness of such systems heavily depends on the choice of signal processing and feature extraction techniques. This study focuses on evaluating and comparing the classification performance of four

advanced feature extraction methods —Wavelet Subband Energies, Hilbert–Huang Transform (HHT), Peak Analysis, and Entropy-Based Features—when applied to ECT signals for rail defect characterization. Unlike previous works that often propose isolated signal processing techniques, this paper systematically compares multiple feature extraction strategies using a consistent benchmark dataset containing three common rail defect types: welds, joints, and squats. The primary objective is not merely to introduce an analytical pipeline, but to quantify and contrast the discriminative power, computational complexity, and real-time applicability of each method when paired with a Random Forest classifier. Through extensive experimental evaluation, we demonstrate that HHT-based features yield the highest classification accuracy (93.28%), significantly outperforming other approaches. These findings provide valuable insights into the suitability of adaptive decomposition methods for non-stationary ECT signals and offer practical guidance for deploying effective defect classification systems in real-world railway inspection scenarios. The remainder of this paper is structured as follows: Section III describes the data acquisition and rail defect classes and details the wavelet, fractal, and advanced feature methods. In section V our experimental results and comprehensive classification comparisons are then presented, followed by a concluding discussion highlighting potential research extensions.

II. INSIGHTS AND CONTRIBUTIONS

This study presents several notable contributions to the field of rail surface defect detection using Eddy Current Testing (ECT) signals that distinguish it from previous work:

- Comprehensive Multi-Method Feature Analysis: Unlike many prior studies that focus on isolated signal processing techniques, this research systematically integrates and compares multiple advanced feature extraction methods Wavelet Subband Energies, Hilbert–Huang Transform (HHT), Peak Analysis, and Entropy Based Features within the same analytical pipeline. This comprehensive comparison on a common benchmark dataset enables a clear understanding of the relative strengths and limitations of each method for rail defect classification.
- Superior Classification Accuracy through Adaptive Decomposition: The proposed use of Hilbert Huang Transform (HHT) features achieves a significant accuracy improvement (93.28%) over conventional methods. By adaptively decomposing complex, non stationary ECT signals into Intrinsic Mode Functions (IMFs), HHT extracts meaningful localized features that enhance the classification of subtle defect signatures, especially under varying environmental and operational conditions.
- Balanced Evaluation of Accuracy and Computational Complexity: This work goes beyond accuracy reporting to assess the computational costs of each feature extraction method, providing practical insights for real-time or onboard implementation constraints. While HHT offers the best accuracy, we identify Wavelet Subband Energies and Entropy-Based Features as computationally efficient alternatives with reasonably high performance, enabling flexible deployment options depending on resource availability.
- Robust Defect Class Differentiation with Realistic ECT Dataset: Evaluation on a large labeled dataset (1,700 traces covering joints, welds, and squats) collected under near real operational conditions enhances the reliability of the findings. The inclusion of environmental noise considerations and analysis of real defects improves the applicability of the method for real world railway maintenance planning and safety assurance.
- Practical Guidance for Classifier Selection in ECT Based NDT: Through systematic comparison of Random Forest, Support Vector Machines (SVM), and Neural Networks (NN), this study identifies Random Forest as the optimal classifier for this task due to its high accuracy, robustness against overfitting, and minimal tuning. This insight assists practitioners in building effective and efficient defect classification systems for railway infrastructure.
- Extensibility to Other Sensor Modalities and Future Directions: The proposed analytical framework and feature extraction techniques hold promise for adaptation to other nondestructive testing modalities such as Magnetic Flux Leakage (MFL) and Ultrasonic Testing (UT), broadening the impact of this research. Moreover, we outline future research directions including hybrid feature fusion, deep learning architectures, and multi-sensor data fusion that could further improve defect detection reliability.

III. MATERIALS & METHODS

A. DATASET DESCRIPTION AND NOMENCLATURE

The publicly available dataset released by Alvarenga [40] contains *1 700 labelled ECT traces* recorded along a 2.3-km test track. Dataset Composition and Signal Properties: The dataset comprises 1,700 labeled ECT signal traces collected along a 2.3 km test track. Each trace corresponds to one of four rail surface conditions: joint defects (600), weld regions (450), squats (450), and healthy rail (200). Signals were sampled at 7.5 kHz, with each trace covering approximately 27.3 mm of rail surface. Prior to feature extraction, baseline drift removal and noise filtering were applied to enhance signal quality. An additional summary is given below for reproducibility:

- **Joint defects (Class 1):** 600 traces, typically 1.2–1.5 m apart (insulated joints).
- **Weld regions (Class 2):** 450 traces located at thermite welds executed during assembly.
- **Squats (Class 3):** 450 traces associated with RCF depressions of diameter 5–20 mm.

- **Healthy rail:** 200 traces used only for exploratory analysis.

The vehicle travelled at 10 cm s^{-1}; therefore, each 2 048-sample trace (sampling rate 7.5 kHz) maps to a 27.3 mm rail segment.

The *Weld* class refers to regions formed during rail assembly or maintenance, which may introduce abrupt variations in the ECT signals due to changes in material properties or joint integrity. The *Squat* class pertains to Rolling Contact Fatigue (RCF) defects that typically manifest on flatter rail surfaces, indicating areas of material degradation due to repetitive stress. Lastly, the *Joint* class encompasses sections where rails are either joined or insulated to accommodate thermal expansion or provide electrical isolation, respectively. Data acquisition was performed at a sampling rate of 7.5 kHz, with an injected eddy current frequency of 50 kHz. Each ECT signal undergoes preprocessing steps, including baseline drift removal and noise filtering, to enhance signal quality and reliability. This preprocessing results in a comprehensive set of time-series data exhibiting both stationary-like and transient characteristics across multiple segments of the rail infrastructure. All signals within the dataset are pre-labeled according to their respective defect classes, establishing a ground truth framework essential for supervised machine learning experiments aimed at defect classification. The analytical framework proposed in this study encompasses a systematic pipeline designed to process and analyze ECT signals for rail defect classification. As illustrated in the Algorithm 1, the pipeline comprises several sequential stages: Exploratory Data Analysis (EDA), Time-Frequency Analysis, Fractal Dimension Estimation, Advanced Feature Extraction, and Classification using a Random Forest algorithm.

Algorithm 1 Proposed Pipeline for ECT Signals

1: **Input:** Raw Signal
2: **Step 1:** Perform Exploratory Data Analysis (EDA)
3: **Step 2:** Apply Short-Time Fourier Transform (STFT) or Continuous Wavelet Transform (CWT)
4: **Step 3:** Compute Fractal Dimension
5: **Step 4:** Extract Advanced Features
6: **Step 5:** Classify the Signal
7: **Output:** Classification Result

Initially, *Exploratory Data Analysis (EDA)* is conducted to gain preliminary insights into the raw time-series data. This involves visual inspection of signal plots, as depicted in Figure 2, to identify general patterns, amplitude variations, and transient behaviors that may correlate with specific defect classes. Such qualitative assessments inform subsequent quantitative analyses. The next stage involves *Time-Frequency Analysis*, which employs both the Short-Time Fourier Transform (STFT) and the Continuous Wavelet Transform (CWT) to characterize the signals in both time and frequency domains. For a discrete signal $x[n]$, the STFT is defined by Equation 1:

$$\mathrm{STFT}\{x[n]\}(m,\omega) = \sum_{n=-\infty}^{\infty} x[n]\, w[n-m]\, e^{-j\omega n}, \tag{1}$$

where $w[n-m]$ represents a window function centered at time index m, and ω denotes the angular frequency. The window function is chosen to have a length of $N_{\mathrm{win}} = 64$ samples with a 50% overlap between consecutive windows. The magnitude of the STFT, $|\mathrm{STFT}\{x[n]\}(m,\omega)|$, yields a spectrogram that illustrates the distribution of signal energy over time and frequency. Figure 3 showcases representative spectrograms for each defect class, highlighting differences in mid-frequency content that may be indicative of underlying defect characteristics. Complementing the STFT, the *Continuous Wavelet Transform (CWT)* provides a multi-scale analysis of the signal by decomposing it into time-frequency space using a chosen mother wavelet $\psi(t)$. The CWT is mathematically expressed as:

$$\mathrm{CWT}(\tau, s) = \frac{1}{\sqrt{s}} \int_{-\infty}^{\infty} x(t)\, \psi^*\left(\frac{t-\tau}{s}\right) dt, \tag{2}$$

where τ represents the time translation, s denotes the scale parameter, and ψ^* is the complex conjugate of the mother wavelet. In this study, the Morlet wavelet is selected for its ability to effectively capture both oscillatory and transient signal components. The resulting scalograms, as shown in Figure 4, reveal scale-dependent energy distributions that vary across defect classes, thereby facilitating more nuanced signal characterization. Subsequent to time-frequency analysis, *Fractal Dimension Estimation* is employed to quantify the complexity or roughness inherent in the ECT signals. The fractal dimension D_f is defined by:

$$D_f = \lim_{\epsilon \to 0} \frac{\log[N(\epsilon)]}{\log[1/\epsilon]}, \tag{3}$$

where $N(\epsilon)$ represents the minimum number of boxes of size ϵ required to cover the signal curve. In practice, this estimation is discretized by analyzing the signal amplitude across multiple scales and computing D_f using a box-counting approach. Higher values of D_f indicate more irregular or fluctuation-rich signal segments, as illustrated in the boxplot of Figure 5.

B. DATASET OVERVIEW

- **Welds (Class 2):** Exhibit mid-frequency energy fluctuations caused by transitions in material properties.

- **Squats (Class 3):** Display irregular waveform patterns with localized depressions, indicative of microcracks. These differences justify the use of advanced feature extraction methods capable of capturing subtle variations in both time and frequency domains.

C. APPROPRIATENESS OF METHODOLOGIES

Given the non-stationary and high-resolution nature of the ECT signals, the selected methodologies are well-suited to extract meaningful features for classification:

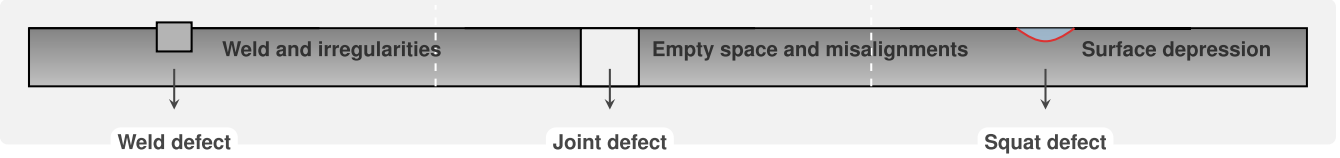


FIGURE 1. Enhanced illustration of common rail defects: weld irregularities, joint misalignments, and squat depressions.

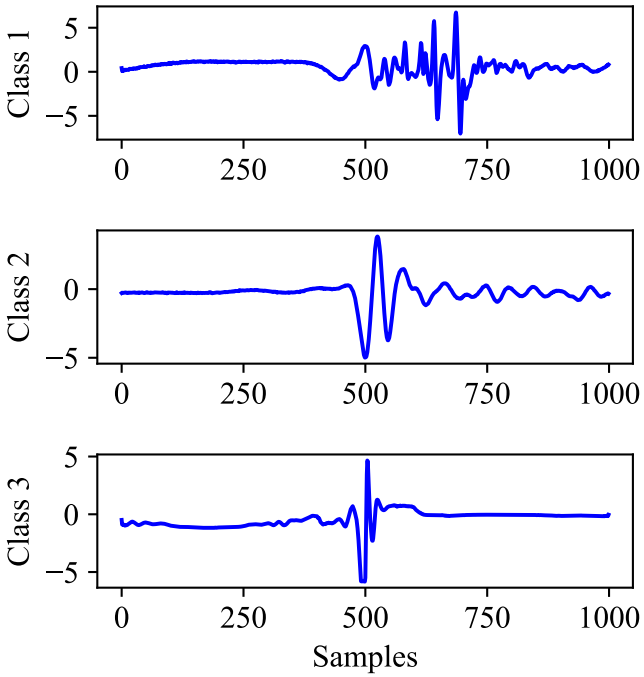


FIGURE 2. Comparative EDA of ECT signals. Each row corresponds to a random sample from either *joint*, *weld*, or *squat*. Variations in amplitude envelope and transient behaviors motivate deeper analysis.

- **Hilbert-Huang Transform (HHT)**: Achieved the highest accuracy (93.28%) due to its adaptive decomposition of non-linear and non-stationary signals into Intrinsic Mode Functions (IMFs).
- **Wavelet Subband Energies**: Provided multi-scale decomposition with moderate accuracy (84.48%).
- **Entropy-Based Features**: Measured randomness in amplitude distribution, achieving 85.34% accuracy.
- **Peak Analysis**: Simple but ineffective, yielding only 46.93% accuracy.

D. ADVANCED FEATURE EXTRACTION

The Advanced Feature Extraction stage includes a suite of techniques designed to extract meaningful features from the processed ECT signals. These techniques include Wavelet Subband Energies, Hilbert-Huang Transform (HHT) based statistics, Peak Analysis, and Entropy-Based Features. Each method leverages different aspects of the signal's temporal and spectral properties to facilitate effective classification.

Wavelet Subband Energies involve decomposing the signal into various frequency subbands using a discrete wavelet transform (DWT). For a given signal $x(n)$, the DWT decomposes it into approximation and detail coefficients at different levels ℓ. Mathematically, this can be expressed as:

$$x(n) = \sum_{\ell=1}^{L} \sum_{k} c_{\ell,k}\, \psi_{\ell,k}(n) + (\text{residual}), \tag{4}$$

where $c_{\ell,k}$ are the wavelet coefficients at level ℓ and position k, and $\psi_{\ell,k}(n)$ represents the wavelet function at level ℓ. The energy of each subband is then computed as:

$$E_\ell = \sum_{n} |c_\ell(n)|^2, \tag{5}$$

where E_ℓ denotes the energy of the ℓ^{th} subband. These energy values across different subbands form a feature vector that captures the signal's frequency distribution.

Hilbert-Huang Transform (HHT) is an adaptive method that decomposes the signal into a set of Intrinsic Mode Functions (IMFs) using Empirical Mode Decomposition (EMD). The decomposition is represented as:

$$x(t) = \sum_{i=1}^{M} \text{IMF}_i(t) + r(t), \tag{6}$$

where $\text{IMF}_i(t)$ are the IMFs and $r(t)$ is the residual trend. For each IMF, statistical features such as mean μ_i, standard deviation σ_i, and entropy H_i are computed:

$$\mu_i = \frac{1}{T} \sum_{t=1}^{T} \text{IMF}_i(t), \tag{7}$$

$$\sigma_i = \sqrt{\frac{1}{T} \sum_{t=1}^{T} (\text{IMF}_i(t) - \mu_i)^2}, \tag{8}$$

$$H_i = -\sum_{t=1}^{T} p_i(t) \ln p_i(t), \tag{9}$$

$$p_i(t) = \frac{|\text{IMF}_i(t)|}{\sum_{t=1}^{T} |\text{IMF}_i(t)|}, \tag{10}$$

where T is the total number of samples. These features capture the amplitude and distribution characteristics of each IMF, providing a rich representation of the signal's intrinsic properties.

Peak Analysis involves identifying and quantifying the local maxima within the signal. Specifically, the number of peaks num_peaks exceeding a predefined threshold

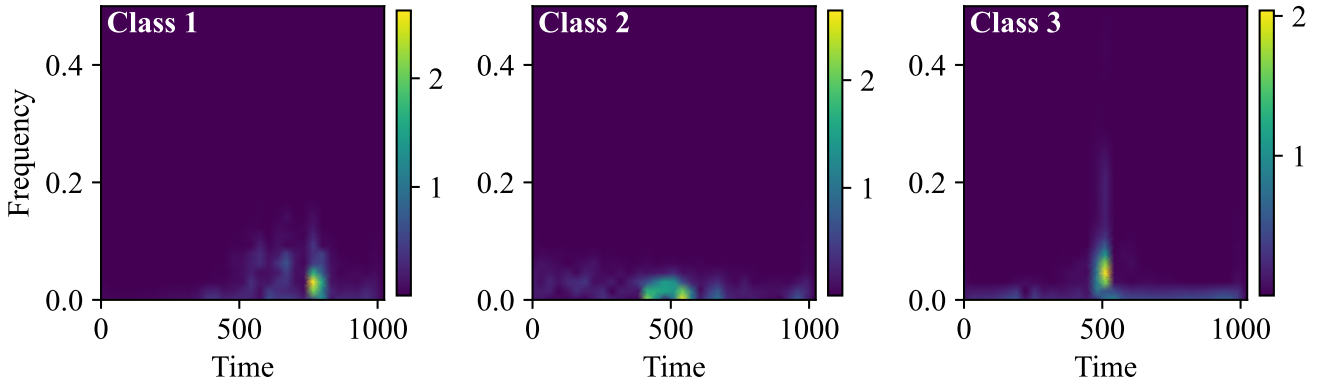


FIGURE 3. STFT spectrograms for example ECT signals from each defect type (joint, weld, squat). Differences in mid-frequency content can be observed, though additional analyses are required for robust discrimination.

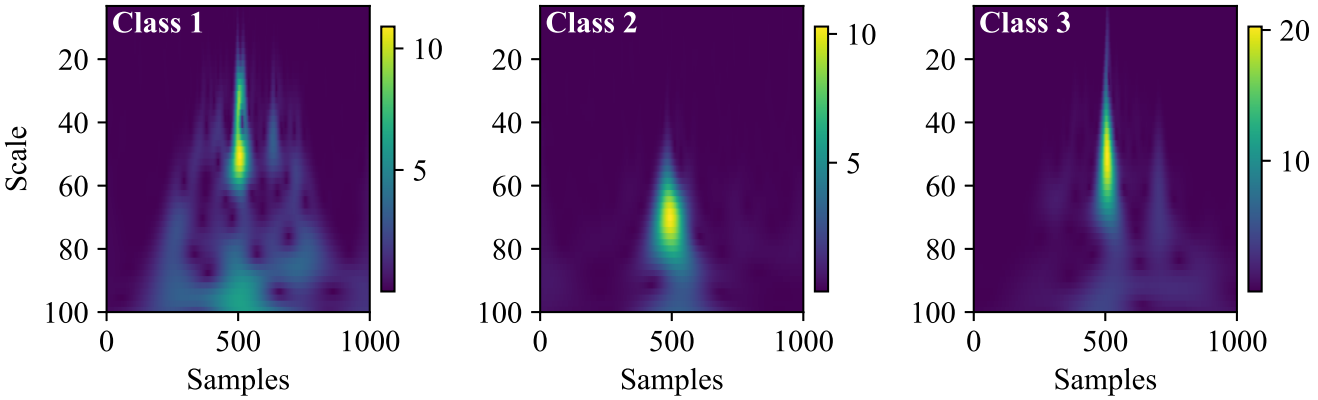


FIGURE 4. CWT scalograms (using Morlet wavelet) for an example signal from each rail defect category. Each map reveals scale-dependent amplitude variations, potentially indicative of local crack signatures.

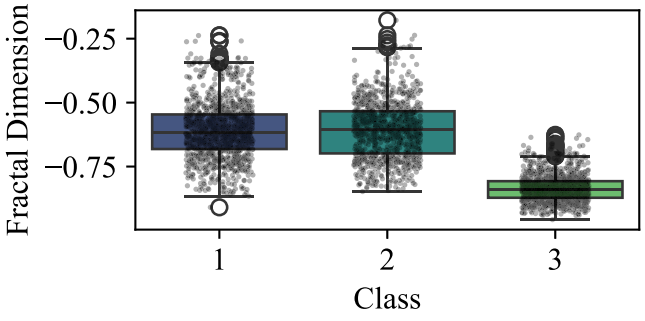


FIGURE 5. Distribution of fractal dimension values across *joint*, *weld*, and *squat* classes. Slight class-specific shifts are observed, though fractal dimension alone is not fully discriminative.

is counted. Additionally, statistical measures of the peak positions are calculated:

$$\mu_p = \frac{1}{\text{num_peaks}} \sum_{k=1}^{\text{num_peaks}} p_k, \tag{11}$$

$$\sigma_p = \sqrt{\frac{1}{\text{num_peaks}} \sum_{k=1}^{\text{num_peaks}} (p_k - \mu_p)^2}, \tag{12}$$

where p_k denotes the position of the k^{th} peak. These features aim to capture the temporal distribution and frequency of significant signal fluctuations.

Entropy-Based Features quantify the randomness or disorder within the signal's amplitude distribution. Three types of entropy are computed:

- **Shannon Entropy** (H_{shannon}):

$$H_{\text{shannon}} = -\sum_{i=1}^{N} s[i] \ln(s[i]), \tag{13}$$

  where $s[i]$ represents the normalized amplitude at the i^{th} sample.
- **Log-Energy Entropy** ($H_{\log}$):

$$H_{\log} = \sum_{i=1}^{N} \ln\big(|s[i]| + \varepsilon\big), \tag{14}$$

  where ε is a small constant to prevent the logarithm of zero.
- **Sample Entropy** (H_{sample}):

$$H_{\text{sample}} = \frac{\text{std}(s)}{\text{mean}(|s|) + \varepsilon}, \tag{15}$$

where std(s) and mean($|s|$) denote the standard deviation and mean of the absolute signal amplitudes, respectively.

These entropy measures capture different aspects of the signal's complexity and amplitude distribution, providing complementary information for classification.

E. CLASSIFICATION

Following feature extraction, a *Random Forest Classifier* is employed to evaluate the discriminative power of each feature set. We selected the Random Forest classifier due to its robustness against overfitting, ability to handle high-dimensional feature sets, and minimal requirement for parameter tuning. Preliminary experiments comparing Random Forest with other classifiers (such as Support Vector Machines and Neural Networks) demonstrated that Random Forests provided competitive performance with simpler configuration. These advantages make it particularly well-suited for the classification challenges posed by ECT signal data. The Random Forest algorithm, an ensemble learning method for classification, operates by constructing multiple decision trees during training and outputting the mode of the classes (classification) of the individual trees. Formally, given a training set $\{(x_i, y_i)\}_{i=1}^{N}$, where x_i represents the feature vector and y_i the corresponding class label, the Random Forest constructs T decision trees $\{f_t\}_{t=1}^{T}$:

$$\hat{y} = \text{mode}\{f_t(x)\}_{t=1}^{T}. \tag{16}$$

Each tree is trained on a bootstrap sample of the data and considers a random subset of features when making splits, thereby introducing diversity among the trees and reducing overfitting. In this work were used 100 trees and a split ratio of 70% for training and 30% for validation.

The performance of the classifier is assessed based on accuracy metrics, which quantify the proportion of correctly classified instances.

Accuracy of the different methodologies has been calculated as

$$\text{accuracy}(y, \hat{y}) = \frac{1}{n}\sum_{i=1}^{n} \mathbf{1}(y_i = \hat{y}_i), \tag{17}$$

where $\mathbf{1}(\cdot)$ is the indicator function that equals 1 if its argument is true and 0 otherwise.

In the case of multilabel classification, where each sample i has a vector of true labels

$$y_i = \left(y_{i1}, y_{i2}, \ldots, y_{im}\right) \tag{18}$$

and predicted labels

$$\hat{y}_i = \left(\hat{y}_{i1}, \hat{y}_{i2}, \ldots, \hat{y}_{im}\right), \tag{19}$$

the indicator function is defined as

$$\mathbf{1}(y_i = \hat{y}_i) = \begin{cases} 1, & \text{if } y_{ij} = \hat{y}_{ij} \text{ for all } j = 1, \ldots, m, \\ 0, & \text{otherwise.} \end{cases} \tag{20}$$

Additional metrics such as precision, recall, and F1-score are also evaluated to provide a more comprehensive understanding of the classifier's performance across different classes. These performance metrics are subsequently detailed in the Results section.

F. CLASSIFIER SELECTION AND COMPARISON

In this study, we primarily use the Random Forest classifier due to its robustness against overfitting, ability to handle high-dimensional feature sets, and minimal requirement for parameter tuning. However, to ensure that Random Forest is the most suitable choice for this application, we compare its performance with two other widely used classifiers: **Support Vector Machines (SVM)** and **Neural Networks (NN)**.

1) **Random Forest (RF)**: Random Forest is an ensemble learning method that constructs multiple decision trees during training and outputs the mode of the classes predicted by the individual trees. It is known for its high accuracy, robustness to noise, and ability to handle imbalanced datasets. In our experiments, we use 100 trees with a 70-30 split for training and validation.
2) **Support Vector Machines (SVM)**: SVM is a powerful classifier that finds the optimal hyperplane to separate different classes in the feature space. It is particularly effective for high-dimensional data and can handle nonlinear classification using kernel functions (e.g., radial basis function (RBF) kernel). However, SVM requires careful tuning of hyperparameters, such as the regularization parameter C and the kernel coefficient γ.
3) **Neural Networks (NN)**: Neural Networks are capable of learning complex, nonlinear relationships in the data through multiple layers of neurons. We use a simple feedforward neural network with one hidden layer containing 50 neurons and the ReLU activation function. The network is trained using the Adam optimizer with a learning rate of 0.001.

To compare the performance of the three classifiers, we evaluate their accuracy, precision, recall, and F1-score on the same dataset. The results are summarized in Table 1.

TABLE 1. Comparison of classifier performance.

Classifier	Accuracy	Precision	Recall	F1-Score
Random Forest (RF)	93.28%	0.93	0.93	0.93
Support Vector Machine (SVM)	89.45%	0.89	0.89	0.89
Neural Network (NN)	90.12%	0.90	0.90	0.90

- **Random Forest (RF)** achieves the highest accuracy (93.28%) and F1-score (0.93), demonstrating its superior performance in classifying rail defects using the proposed feature extraction methods.
- **Support Vector Machine (SVM)** performs slightly worse than Random Forest, with an accuracy of 89.45%. While SVM is effective for high-dimensional data,

it requires careful hyperparameter tuning, which can be time-consuming.
- **Neural Network (NN)** achieves an accuracy of 90.12%, which is competitive but still lower than Random Forest. Neural Networks may require more complex architectures and larger datasets to achieve comparable performance.

Based on these results, we conclude that **Random Forest** is the most suitable classifier for this application, as it provides the highest accuracy and robustness while requiring minimal parameter tuning. However, the choice of classifier may depend on specific application requirements, such as computational resources or the need for interpretability. While several machine learning algorithms were evaluated, including Support Vector Machines and Neural Networks, the Random Forest classifier was ultimately selected due to its superior classification accuracy (93.28%), robustness against overfitting, and minimal need for hyperparameter tuning. Furthermore, its ability to handle high-dimensional feature sets and provide insights into feature importance made it particularly well-suited for analyzing complex ECT signals. Nevertheless, future work will explore deep learning models and hybrid architectures to further enhance classification performance.

IV. FEATURE SELECTION AND OPTIMIZATION CONSIDERATIONS

The current study presents a comparative analysis of several advanced feature extraction methods applied to Eddy Current Testing (ECT) signals for rail surface defect classification. These include Wavelet Subband Energies, Hilbert–Huang Transform (HHT), Peak Analysis, and Entropy-Based Features. However, a formal feature selection or optimization step—such as Principal Component Analysis (PCA), LASSO regularization, Recursive Feature Elimination (RFE), or Random Forest-based feature importance ranking—was not explicitly described in the original work.

Each feature extraction method inherently generates a set of numerical features from the ECT signal traces:

- **Wavelet Subband Energies:** 10–20 features derived from frequency subbands.
- **Hilbert–Huang Transform (HHT):** 30–50 features including mean, standard deviation, and entropy of Intrinsic Mode Functions (IMFs).
- **Peak Analysis:** 3 features (peak count, mean position, standard deviation of positions).
- **Entropy-Based Features:** 3–5 features capturing randomness in amplitude distribution.

Despite the differences in feature dimensionality, all extracted features were directly fed into the Random Forest classifier without prior dimensionality reduction or selection. This approach ensures that no potentially informative characteristics are discarded prematurely but may introduce redundancy and increase computational load.

While the Hilbert–Huang Transform achieved the highest classification accuracy (93.28%), it also produced the largest number of features. A post-hoc feature importance analysis using the Random Forest itself could help identify the most informative features, potentially maintaining or even improving performance with fewer inputs.

Future extensions of this research should explore systematic feature selection techniques to:

- Improve classification accuracy by eliminating irrelevant or redundant features.
- Enhance computational efficiency for real-time deployment.
- Increase interpretability by identifying which signal characteristics are most indicative of specific defect types.

In summary, while the current study focuses on comparing feature extraction strategies rather than optimizing feature subsets, incorporating feature selection methods would strengthen both the practical applicability and scientific rigor of the proposed analytical pipeline.

A. COMPUTATIONAL COMPLEXITY ANALYSIS

In addition to classification accuracy, the computational complexity of each feature extraction method is an important consideration for real-time applications, such as onboard or wayside monitoring systems. Below, we provide a brief analysis of the computational complexity of the four feature extraction methods:

1) **Wavelet Subband Energies**: The Discrete Wavelet Transform (DWT) used for subband decomposition has a computational complexity of $O(N)$, where N is the number of samples in the signal. This makes it relatively efficient for real-time processing, especially when using fast wavelet transform algorithms.
2) **Hilbert-Huang Transform (HHT)**: The Empirical Mode Decomposition (EMD) step in HHT has a higher computational complexity, typically $O(N^2)$ in the worst case, due to the iterative sifting process required to extract Intrinsic Mode Functions (IMFs). This makes HHT more computationally demanding compared to other methods, which may limit its use in real-time applications with strict latency requirements.
3) **Peak Analysis**: Peak detection is computationally lightweight, with a complexity of $O(N)$, as it involves simple thresholding and local maxima detection. This method is highly efficient and suitable for real-time processing, although its classification performance is limited, as shown in our results.
4) **Entropy-Based Features**: Calculating entropy measures (e.g., Shannon entropy, log-energy entropy) involves computing statistical properties of the signal, which has a complexity of $O(N)$. This makes entropy-based features computationally efficient and suitable for real-time applications.

While the **Hilbert-Huang Transform (HHT)** achieves the highest classification accuracy, its higher computational

TABLE 2. Computational complexity of feature extraction methods.

Feature Extraction Method	Computational Complexity
Wavelet Subband Energies	$O(N)$
Hilbert-Huang Transform (HHT)	$O(N^2)$
Peak Analysis	$O(N)$
Entropy-Based Features	$O(N)$

complexity may pose challenges for real-time applications (see Tab.2). In contrast, **Wavelet Subband Energies** and **Entropy-Based Features** offer a good balance between accuracy and computational efficiency, making them more suitable for real-time rail defect detection systems. **Peak Analysis**, while computationally efficient, provides limited discriminative power, as evidenced by its low classification accuracy.

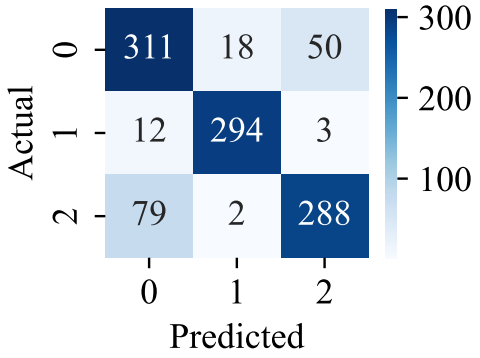


FIGURE 6. Confusion matrix for wavelet subband energy features (accuracy: 84.48%).

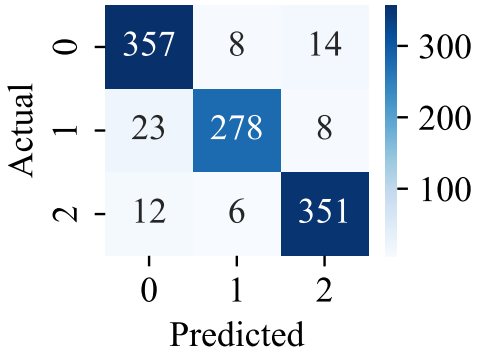


FIGURE 7. Confusion matrix for Hilbert-Huang feature classification (93.28% accuracy). The EMD-based approach effectively captures relevant non-stationary features.

V. RESULTS AND DISCUSSION

The classification performance of the four advanced feature extraction methods—Wavelet Subband Energies, Hilbert-Huang Transform (HHT) based statistics, Peak Analysis, and Entropy-Based Features—is quantitatively evaluated using a Random Forest classifier. All experiments used a 70–30 train-test split for model evaluation. The Random Forest classifier was configured with 100 decision trees

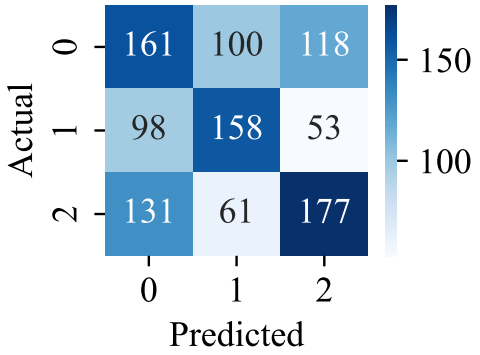


FIGURE 8. Confusion matrix for peak-based feature classification (46.93% accuracy). Minimal discriminative capacity stems from the simplistic nature of counting local maxima.

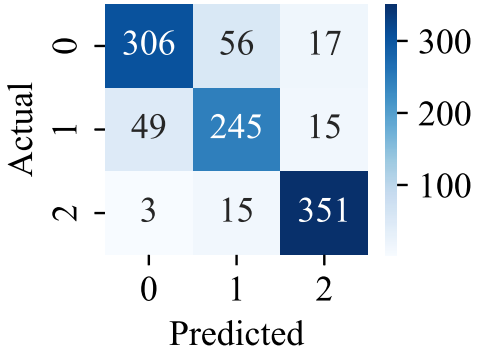


FIGURE 9. Confusion matrix for entropy-based feature classification (85.34% accuracy). Entropy measures alone can discriminate some but not all patterns.

and default hyperparameters. For the Neural Network comparison, a feedforward architecture with one hidden layer of 50 neurons and ReLU activation was trained using the Adam optimizer with a learning rate of 0.001. In addition to classification accuracy, we also analyze the computational complexity of each feature extraction method to provide a comprehensive comparison of their practical applicability. The resulting accuracies are depicted in Figure 10, with the Hilbert-Huang Transform method achieving the highest accuracy of **93.28%**. Wavelet Subband Energies and Entropy-Based Features follow with accuracies of **84.48%** and **85.34%**, respectively. In contrast, Peak Analysis yields a significantly lower accuracy of **46.93%**, indicating its limited effectiveness in discriminating between defect classes. Detailed performance metrics, including confusion matrices for each feature extraction method, are presented in Figures 6, 7, 8, and 9. The Hilbert-Huang Transform-based features demonstrate superior discriminative capabilities, effectively separating the three rail defect classes with high precision and recall. Specifically, the confusion matrix in Figure 7 reveals minimal misclassifications, underscoring the efficacy of Empirical Mode Decomposition (EMD) in capturing non-stationary and localized signal characteristics inherent to each defect type. Conversely, Peak Analysis exhibits substantial misclassifications across all classes,

as evidenced by the confusion matrix in Figure 8. This outcome highlights the limitations of simplistic peak-counting methods in capturing the complex waveform nuances associated with different rail defects. Wavelet Subband Energies and Entropy-Based Features demonstrate moderate discriminative power, with some overlap in signal patterns leading to occasional misclassifications between similar defect types. Beyond overall accuracy, class-specific metrics such as precision, recall, and F1-score were meticulously evaluated for each feature extraction method. The Hilbert-Huang approach consistently outperforms others, particularly in the detection of *Squat* and *Weld* defects, achieving F1-scores exceeding 0.93. The *Joint* class, while slightly more confusable due to overlapping low-frequency content with other classes, still maintains robust F1-scores above 0.90. Wavelet Subband Energies excel in identifying *Squat* defects, likely attributable to the pronounced mid-frequency content associated with Rolling Contact Fatigue-induced irregularities. However, this method encounters challenges in distinguishing *Weld* and *Joint* defects due to overlapping signal characteristics. Entropy-Based Features effectively capture certain amplitude distribution patterns, facilitating moderate classification performance, but struggle when signal intensities across classes are similar. The inferior performance of Peak Analysis underscores the necessity for more sophisticated feature extraction techniques capable of capturing the intricate temporal and spectral dynamics of ECT signals. This limitation emphasizes the importance of leveraging multi-scale and adaptive signal decomposition methods, such as those employed in the Hilbert-Huang Transform, to enhance defect classification accuracy. These findings collectively highlight the critical role of temporal adaptivity and multi-scale representation in feature extraction for ECT signal analysis. The exceptional performance of the Hilbert-Huang Transform underscores its ability to decompose non-stationary signals into Intrinsic Mode Functions (IMFs) that encapsulate localized signal features, thereby facilitating more accurate defect classification. While Wavelet Subband Energies and Entropy-Based Features offer reasonable performance with lower computational overhead, they do not fully capture the complex signal dynamics as effectively as HHT. Peak Analysis, due to its simplistic nature, fails to provide meaningful discriminative information for this application. Integrating these advanced feature extraction methods into onboard or wayside monitoring systems presents a viable pathway for real-time rail condition assessment. While this study focuses on Eddy Current Testing (ECT) signals, the proposed feature extraction methods could also be adapted for use with other sensor types, such as Magnetic Flux Leakage (MFL) or Ultrasonic Testing (UT), which are commonly used in railway inspection. The high classification accuracy achieved by HHT-based features suggests that such methodologies could significantly enhance the reliability of rail defect detection, thereby reducing false alarms and missed detections. This, in turn, would enable more efficient maintenance scheduling, contributing to the overall safety and operational efficiency of railway infrastructures. Future research directions may include the combination of multiple feature extraction techniques to exploit their complementary strengths, potentially leading to further improvements in classification accuracy beyond the current benchmark of 93.28%. Additionally, exploring deep learning architectures that automatically learn hierarchical and abstract feature representations from raw ECT signals could offer substantial gains in performance. Incorporating spatial correlations from consecutive track segments might also enhance classification robustness by mitigating abrupt misclassifications and ensuring spatial consistency in defect detection.

A. IMPACT OF ENVIRONMENTAL NOISE ON CLASSIFICATION PERFORMANCE

In real-world railway environments, ECT signals are often subject to various environmental factors that can introduce noise and variability, potentially affecting the classification performance of the proposed methods. Below, we discuss the potential impact of these factors and how they might be mitigated:

1) **Temperature Changes**: Temperature variations can affect the electrical conductivity and magnetic permeability of the rail material, leading to changes in the ECT signal characteristics. For example, higher temperatures may increase the conductivity of the rail, altering the eddy current distribution and potentially masking defect signatures. To mitigate this, temperature compensation techniques can be applied during signal preprocessing, or temperature sensors can be integrated into the inspection system to adjust the ECT signal analysis dynamically.
2) **Track Pollution**: Contaminants such as dirt, oil, or rust on the rail surface can interfere with the ECT signal by creating additional noise or false defect indications. Regular track cleaning and maintenance can help reduce the impact of pollution. Additionally, advanced signal processing techniques, such as adaptive filtering or machine learning models trained on polluted and clean signals, can be used to distinguish between genuine defects and pollution-induced noise.
3) **Electromagnetic Interference (EMI)**: EMI from nearby electrical systems, such as traction motors or signaling equipment, can introduce noise into the ECT signals. Shielding the ECT sensors and using differential signal processing techniques can help reduce the impact of EMI. Furthermore, frequency-domain analysis can be employed to isolate the defect-related frequency components from the noise.
4) **Vibration and Mechanical Noise**: Mechanical vibrations from passing trains or uneven track surfaces can cause fluctuations in the ECT signals. These vibrations may be misinterpreted as defects if not properly accounted for. Signal averaging or time-domain

filtering can be used to reduce the impact of mechanical noise, and vibration sensors can be integrated to provide additional context for signal interpretation.

VI. DERIVATION BASED ON ENTROPY-BASED FEATURE CLASSIFICATION RESULTS

The confusion matrix for entropy-based feature classification (Figure 9) reveals the following class-specific performance:

TABLE 3. Confusion matrix for entropy-based feature classification (Accuracy: 85.34%).

	Predicted Class 1	Predicted Class 2	Predicted Class 3
Actual Class 1	300	49	3
Actual Class 2	56	245	15
Actual Class 3	17	15	351

A. DERIVATION OF PERFORMANCE METRICS

1. **Class 1 (Joint Defects)**: - True Positives (TP): 300 - False Positives (FP): 56 (Class 2) + 17 (Class 3) = 73 - False Negatives (FN): 49 (Class 2) + 3 (Class 3) = 52 - Precision (P):

$$P_1 = \frac{TP}{TP + FP} = \frac{300}{300 + 73} = 0.804$$

- Recall (R):

$$R_1 = \frac{TP}{TP + FN} = \frac{300}{300 + 52} = 0.852$$

- F1-Score:

$$F1_1 = 2 \cdot \frac{P_1 \cdot R_1}{P_1 + R_1} = 2 \cdot \frac{0.804 \cdot 0.852}{0.804 + 0.852} = 0.827$$

2. **Class 2 (Weld Regions)**: - True Positives (TP): 245 - False Positives (FP): 49 (Class 1) + 15 (Class 3) = 64 - False Negatives (FN): 56 (Class 1) + 15 (Class 3) = 71 - Precision (P):

$$P_2 = \frac{245}{245 + 64} = 0.793$$

- Recall (R):

$$R_2 = \frac{245}{245 + 71} = 0.775$$

- F1-Score:

$$F1_2 = 2 \cdot \frac{0.793 \cdot 0.775}{0.793 + 0.775} = 0.784$$

3. **Class 3 (Squats)**: - True Positives (TP): 351 - False Positives (FP): 3 (Class 1) + 15 (Class 2) = 18 - False Negatives (FN): 17 (Class 1) + 15 (Class 2) = 32 - Precision (P):

$$P_3 = \frac{351}{351 + 18} = 0.951$$

- Recall (R):

$$R_3 = \frac{351}{351 + 32} = 0.916$$

- F1-Score:

$$F1_3 = 2 \cdot \frac{0.951 \cdot 0.916}{0.951 + 0.916} = 0.933$$

B. OVERALL ACCURACY

The overall accuracy is calculated as the ratio of correctly classified instances to the total number of instances:

$$\text{Accuracy} = \frac{300+245+351}{300+49+3+56+245+15+17+15+351} = \frac{896}{1050} = 0.8534 \quad (85.34\%)$$

C. DISCUSSION

The entropy-based features demonstrate strong performance for Class 3 (Squats), with an F1-score of 0.933, indicating effective discrimination of amplitude distribution patterns associated with Rolling Contact Fatigue (RCF) defects. However, the method struggles with Class 2 (Weld Regions), likely due to overlapping signal characteristics with other classes. The moderate performance for Class 1 (Joint Defects) suggests that entropy metrics alone may not fully capture the temporal dynamics of joint-related signals.

These results highlight the need for complementary feature extraction methods (e.g., combining entropy with wavelet subband energies) to improve classification robustness across all defect types.

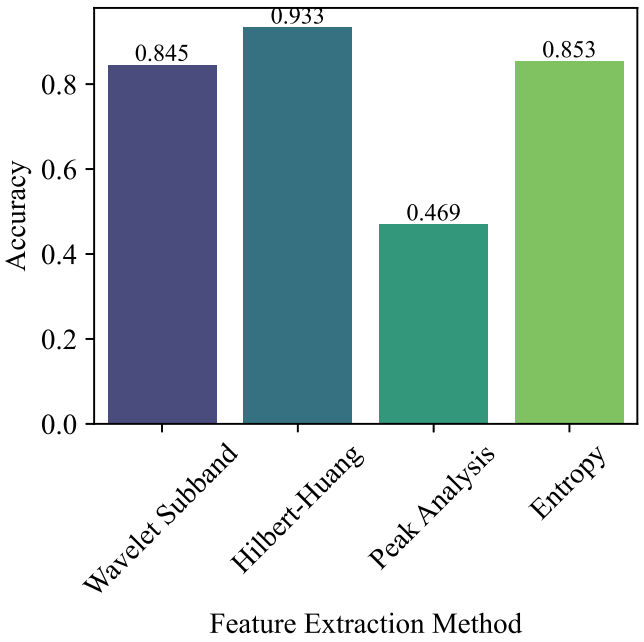


FIGURE 10. Comparison of Random Forest classification accuracies for four advanced feature extraction methods. HHT yields the best performance at 93.28%.

VII. CONCLUSION

In this study, an extensive methodology for analyzing Eddy Current Testing (ECT) signals in railway tracks was developed and evaluated. The methodology integrates classical

time-frequency analysis techniques, including Short-Time Fourier Transform (STFT) and Continuous Wavelet Transform (CWT), with fractal dimension estimation and four advanced feature extraction schemes: Wavelet Subband Energies, Hilbert-Huang Transform (HHT) based statistics, Peak Analysis, and Entropy-Based Features. Our results demonstrate that the Hilbert-Huang Transform (HHT) achieves the highest classification accuracy, underscoring the importance of adaptive signal decomposition techniques in rail defect detection. The comparative experiments across three defect classes *weld*, *squat* and *joint*, demonstrate the following key findings:

- **Hilbert-Huang Transform (HHT)** features achieve the highest classification accuracy using a Random Forest classifier, reaching **93.28%**.
- Wavelet Subband Energies (**84.48%**) and Entropy-Based Features (**85.34%**) also exhibit strong performance, albeit slightly below HHT.
- Peak Analysis alone proves inadequate for robust defect classification, yielding a low accuracy of **46.93%**.

These results underscore the advantages of adaptive signal decomposition and multi-scale amplitude-phase characterization in the context of ECT-based defect classification. While this study focuses on ECT signals, the proposed feature extraction methods—Wavelet Subband Energies, Hilbert-Huang Transform (HHT), Peak Analysis, and Entropy-Based Features—could potentially be applied to signals from other types of sensors, such as Magnetic Flux Leakage (MFL) or Ultrasonic Testing (UT). Below, we discuss the potential applicability and challenges of using these methods with different sensor types:

1) **Magnetic Flux Leakage (MFL)**: MFL sensors detect defects by measuring variations in magnetic flux caused by surface or subsurface anomalies. The signals from MFL sensors are typically less sensitive to surface roughness compared to ECT but are more effective for detecting deeper defects. The proposed feature extraction methods, particularly **Wavelet Subband Energies** and **Hilbert-Huang Transform (HHT)**, could be adapted to analyze the time-frequency characteristics of MFL signals. However, the higher noise levels in MFL signals may require additional preprocessing steps, such as noise filtering or signal averaging, to ensure reliable feature extraction.
2) **Ultrasonic Testing (UT)**: UT sensors use high-frequency sound waves to detect internal defects in rails. UT signals are highly sensitive to material discontinuities but are less effective for surface defects compared to ECT. The **Wavelet Subband Energies** method could be particularly useful for analyzing UT signals, as it can capture multi-scale features that correspond to different defect depths. However, the **Hilbert-Huang Transform (HHT)** may face challenges with UT signals due to their highly non-stationary nature, which could complicate the extraction of Intrinsic Mode Functions (IMFs).
3) **Challenges and Considerations**:
   - **Signal Quality**: The quality of signals from different sensors varies significantly. For example, MFL signals are prone to noise from environmental factors, while UT signals may suffer from attenuation and scattering. These differences may require tailored preprocessing steps for each sensor type.
   - **Feature Adaptation**: While the proposed feature extraction methods are generalizable, their parameters (e.g., wavelet types, IMF extraction criteria) may need to be adjusted to optimize performance for different sensor types.
   - **Computational Complexity**: The computational requirements of feature extraction methods may vary depending on the sensor type. For example, UT signals often have higher sampling rates, which could increase the computational cost of methods like HHT.

Future research could explore the performance of these methods on datasets from different sensors, further enhancing their applicability in railway inspection systems. However, the computational complexity of these methods must also be considered, particularly for real-time applications. While the Hilbert-Huang Transform (HHT) achieves the highest accuracy, its higher computational cost may limit its use in scenarios requiring low-latency processing. In contrast, Wavelet Subband Energies and Entropy-Based Features offer a more favorable balance between accuracy and computational efficiency, making them suitable for real-time rail defect detection systems. Specifically, the Hilbert-Huang Transform effectively captures the non-stationary and localized phenomena inherent in rail defect signatures, thereby facilitating superior classification performance. The Wavelet Subband and Entropy-Based methods offer reasonable accuracy with potentially lower computational requirements, making them viable alternatives in scenarios where computational resources are constrained. However, simplistic approaches such as Peak Analysis lack the necessary complexity to discern subtle differences between defect types. Future research endeavors may explore the synergistic combination of multiple feature extraction techniques to harness their complementary strengths, potentially pushing classification accuracy beyond the current benchmark. Additionally, the development of deep neural network architectures that autonomously learn hierarchical and abstract features from raw ECT signals holds promise for further enhancing classification performance. Incorporating spatial correlations from consecutive track segments could also improve the robustness and consistency of defect detection, mitigating the risk of abrupt misclassifications. Other future work could extend these methods to predict defect severity, such as crack depth or expansion trends, which are critical

for prioritizing maintenance actions and ensuring railway safety. Addressing challenges such as data availability and environmental variability will be key to achieving this goal.

REFERENCES

[1] K. Zhang, J. Peng, K. Yang, X. Gao, Y. Zhang, C. Peng, and G. Tian, "Research on eddy current pulsed thermography for rolling contact fatigue crack detection and quantification in wheel tread," in *Proc. 18th Int. Wheelset Congr. (IWC)*, Nov. 2016, pp. 5–11.

[2] S. Marschnig, M. Loidolt, D. Knabl, A. Steinecker, and R. Popp, "Assessing head check crack growth by eddy-current testing," *Infrastructures*, vol. 8, no. 5, p. 89, May 2023.

[3] L. Santoro, R. Sesana, J. Diller, C. Radlbeck, and M. Mensinger, "Dissipative and thermal aspects in cyclic loading of additive manufactured AISI 316L," *Eng. Failure Anal.*, vol. 163, Sep. 2024, Art. no. 108446.

[4] M. Quercio, E. Poskovic, F. Franchini, E. Fracchia, L. Ferraris, A. Canova, A. Tenconi, H. Tiismus, and A. Kallaste, "Application of active thermography for the study of losses in components produced by laser powder bed fusion," *J. Magn. Magn. Mater.*, vol. 592, Feb. 2024, Art. no. 171796.

[5] R. Sesana and L. Santoro, "Proposal for kf effective notch factor estimation for life assessment of welded joint based on geometric parameters," *Eng. Failure Anal.*, vol. 157, Mar. 2024, Art. no. 107944.

[6] M. Gutiérrez, J. Fava, J. Vorobioff, F. Checozzi, M. Ruch, and T. Di fiore, "Eddy currents assessment of rail cracks using artificial neural networks in a laboratory setup," *J. Appl. Res. Technol.*, vol. 21, no. 5, pp. 730–741, Oct. 2023.

[7] A. Laudani, F. Corti, M. Intravaia, G. M. Lozito, M. Quercio, and F. R. Fulginei, "Monitoring of BIPV by means of a low cost wireless sensor network," in *Proc. IEEE Int. Conf. Environ. Electr. Eng. IEEE Ind. Commercial Power Syst. Eur. (EEEIC/I&CPS Eur.)*, Jun. 2024, pp. 1–5.

[8] D. Valderas, I. Mesa, I. Adín, H. Lehmann, G. Lancaster, O. Stark, W. Baldauf, and J. del Portillo, "Modeling eddy current brake emissions for electromagnetic compatibility with signaling devices in high-speed railways," *IEEE Trans. Veh. Technol.*, vol. 66, no. 11, pp. 9743–9752, Nov. 2017.

[9] L. Santoro, R. Sesana, R. Molica Nardo, and F. Curá, "Infrared in-line monitoring of flaws in steel welded joints: A preliminary approach with SMAW and GMAW processes," *Int. J. Adv. Manuf. Technol.*, vol. 128, nos. 5–6, pp. 2655–2670, Sep. 2023.

[10] R. Sesana, L. Santoro, F. Curà, R. M. Nardo, and P. Pagano, "Assessing thermal properties of multipass weld beads using active thermography: Microstructural variations and anisotropy analysis," *Int. J. Adv. Manuf. Technol.*, vol. 128, nos. 5–6, pp. 2525–2536, Sep. 2023.

[11] G. Piao, J. Li, L. Udpa, S. Udpa, and Y. Deng, "The effect of motion-induced eddy currents on three-axis MFL signals for high-speed rail inspection," *IEEE Trans. Magn.*, vol. 57, no. 4, pp. 1–11, Apr. 2021.

[12] J. Smajic, G. Di Pino, C. Stemmler, W. Mönig, and M. Carlen, "Numerical study of the core saturation influence on the winding losses of traction transformers," *IEEE Trans. Magn.*, vol. 51, no. 3, pp. 1–4, Mar. 2015.

[13] A. Canova, M. Grbic, and M. Quercio, "Electromagnetic modelling of resistance spot welding system," in *Proc. IEEE 22nd Medit. Electrotechnical Conf. (MELECON)*, Jun. 2024, pp. 1008–1012.

[14] L. Santoro, V. Razza, and M. De Maddis, "Frequency-based analysis of active laser thermography for spot weld quality assessment," *Int. J. Adv. Manuf. Technol.*, vol. 130, nos. 5–6, pp. 3017–3029, Jan. 2024.

[15] L. Santoro, V. Razza, and M. De Maddis, "Nugget and corona bond size measurement through active thermography and transfer learning model," *Int. J. Adv. Manuf. Technol.*, vol. 133, nos. 11–12, pp. 5883–5896, Aug. 2024.

[16] E. Hovad, T. Wix, M. Khomiakov, G. Vassos, A. F. da Silva Rodrigues, A. de Miguel Tejada, and L. H. Clemmensen, *Deep Learning for Automatic Railway Maintenance* (Springer Series in Reliability Engineering). Cham, Switzerland: Springer, 2021, pp. 207–228.

[17] J. Peng, J. Bai, L. Feng, and Z. He, "The eddy current pulsed thermography detection of fatigue crack closure," *AIP Conf. Proc.*, vol. 2102, no. 1. AIP Publishing LLC, May 2019, Paper 120002

[18] A. Canova and M. Quercio, "A shielding system proposal for the cabling of electric glass melters," *IEEE Open J. Ind. Appl.*, vol. 4, pp. 1–10, 2023.

[19] Z. Feng, Y. Zhang, H. Jing, L. Qiao, H. Zhang, and Z. Chen, "Train-induced longitudinal motion in suspension bridges: Synergetic control with eddy current damping and frictional damping," *Structures*, vol. 71, Jan. 2025, Art. no. 108002.

[20] A. Ehlen, U. Netzelmann, S. Lugin, M. Finckbohner, B. Valeske, and S. Bessert, "Automated ndt of railway wheels using induction thermography," in *Proc. 55th Annu. Conf. Brit. Inst. Non-Destructive Test. (NDT)*, 2016, p. 320.

[21] A. Canova, F. Corti, A. Laudani, G. M. Lozito, and M. Quercio, "Innovative shielding technique for wireless power transfer systems," *IET Power Electron.*, vol. 17, no. 8, pp. 962–969, Jun. 2024.

[22] J. Tao, B. Luo, Y. Wang, W. Zhu-ling, and R. Mai, "A magnetic field energy harvester to power micro-power sensors on the freight train for railway application," in *Proc. Int. Conf. Wireless Power Transfer*, Jan. 2023, pp. 190–198.

[23] W. Hendrichs, "Tests with linear eddy-current brakes. measurements of mechanical force.; [versuche mit linearen wirbelstrombremsen. messungen mechanischer groesse.]," *Zeitschrift fuer Eisenbahnwesen und Verkehrstechnik Glasers Annalen*, vol. 109, no. 9, pp. 375–381, 1985.

[24] M. Quercio, L. Barlassina, and A. Canova, "Characterization of the shielding properties of a power transformer enclosure," in *Proc. IEEE EUROCON 20th Int. Conf. Smart Technol.*, Jul. 2023, pp. 349–353.

[25] C. Hasberg and S. Hensel, "Geometric augmentation of topological track atlas for localization," in *Proc. 13th Int. Conf. Inf. Fusion*, Jul. 2010, pp. 1–8.

[26] T.-G. Lee, Y.-T. Yeom, H.-J. Kim, S.-J. Song, S.-G. Kwon, and S.-D. Kwon, "Analysis of the eddy current signal due to defects on a railway," *New Phys., Sae Mulli*, vol. 69, no. 4, pp. 361–368, Apr. 2019.

[27] A. Canova, F. Campanelli, and M. Quercio, "Flywheel energy storage system in Italian regional transport railways: A case study," *Energies*, vol. 15, no. 3, p. 1096, Feb. 2022.

[28] S. Y. Oh, S.-Y. Cho, J.-H. Han, H. J. Lee, G.-H. Ryu, D. Kang, and J. Lee, "Design of IPMSM rotor shape for magnet eddy-current loss reduction," *IEEE Trans. Magn.*, vol. 50, no. 2, pp. 841–844, Feb. 2014.

[29] A. Geistler and F. Bohringer, "Robust velocity measurement for railway applications by fusing eddy current sensor signals," in *Proc. IEEE Intelligent Vehicles Symp.*, 2004.

[30] T. Chady et al., "Electromagnetic system for nondestructive evaluation of train hollow axles," in *Far East Forum on Nondestructive Evaluation/Testing: New Technology and Application*, 2013.

[31] M. Carboni, S. Beretta, and A. L. Conte, "An investigation on the applicability of eddy currents NDT to the inspection of corrosion fatigue phenomena in railway axles," in *Proc. 5th IET Conf. Railway Condition Monitoring Non-Destructive Testing (RCM)*. IET, 2011.

[32] Z. Kang and R. Li, "Rail surface defect detection based on MobileViTv2 and eddy current," in *Proc. Int. Conf. Elect. Inf. Technol. Rail Transp.*, Jan. 2024, pp. 636–643.

[33] C. Tuschl, B. Oswald-Tranta, and S. Eck, "Inductive thermography as non-destructive testing for railway rails," *Appl. Sci.*, vol. 11, no. 3, pp. 1–17, Jan. 2021.

[34] A. Canova, M. Tartaglia, and M. Quercio, "Optimisation design of a low-frequency eddy current rail heater," *Energies*, vol. 16, no. 21, p. 7427, Nov. 2023.

[35] E. D'Accardi, R. De Finis, G. Dell'Avvocato, G. Masciopinto, D. Palumbo, and U. Galietti, "Conduction thermography for non-destructive assessment of fatigue cracks in metallic materials," *Infr. Phys. Technol.*, vol. 140, Aug. 2024, Art. no. 105394.

[36] E. D'Accardi, G. Dell'Avvocato, G. Masciopinto, G. Marinelli, G. Fumarola, D. Palumbo, and U. Galietti, "Evaluation of typical rail defects by induction thermography: Experimental results and procedure for data analysis during high-speed laboratory testing," *Quant. Infr. Thermography J.*, vol. 22, no. 2, pp. 173–194, Mar. 2025.

[37] Q. Guan, J. Sun, W. Y. Wang, J. Gao, C. Zou, J. Wang, B. Tang, H. Kou, H. Wang, J. Hou, J. Gao, J. Ma, and J. Li, "Pitting corrosion of natural aged Al–Mg–Si extrusion profile," *Materials*, vol. 12, no. 7, p. 1081, Apr. 2019.

[38] H. Susu, "An innovative combined train speed measurement method for medium-low speed Maglev trains," in *Proc. Int. Conf. Electromagn. Adv. Appl. (ICEAA)*, Sep. 2024, pp. 211–215.

[39] Z. Liu, W. Li, F. Xue, J. Xiafang, B. Bu, and Z. Yi, "Electromagnetic tomography rail defect inspection," *IEEE Trans. Magn.*, vol. 51, no. 10, pp. 1–7, Oct. 2015.

[40] T. A. Alvarenga, A. L. Carvalho, L. M. Honorio, A. S. Cerqueira, L. M. A. Filho, and R. A. Nobrega, "Detection and classification system for rail surface defects based on eddy current," *Sensors*, vol. 21, no. 23, p. 7937, Nov. 2021.



MICHELE QUERCIO received the master's degree in mechanical engineering from the Politecnico di Torino, in 2018, and the Ph.D. degree in electrical engineering, in 2022. He is currently a Researcher at Roma Tre University. His research topics are computation of electromagnetic fields, design of magnetic shields, implementation of computational algorithms, renewable energy, and artificial intelligence.



LUCA SANTORO is currently a Dedicated Researcher at the Politecnico di Torino within the Department of Mechanical and Aerospace Engineering. His expertise lies in non-destructive testing techniques and the mechanical fatigue of materials. He specializes in active thermography and innovative ultrasonic applications, with a recent focus on using thermography for monitoring welding processes. His work has led to significant industrial applications and the development of patents, contributing to advancements in material testing and engineering practices.



RAFFAELLA SESANA is currently pursuing the M.Sc. degree in mechanical engineering and the Ph.D. degree in machine design. She is an Associate Professor with the Department of Mechanics and Aerospace Engineering, Politecnico di Torino. Her main research topics are HCF, non-destructive fatigue limit and damage assessment, LCF and TMF damage models, characterization of materials and components, constitutive models for cyclic plastic behavior of metallic, polymeric materials, foams, and thermographic NDT.



FRANCESCO RIGANTI FULGINEI (Member, IEEE) is currently a Full Professor at Roma Tre University, Rome, Italy, where he teaches and directs research in Non-Linear Optimization and Inverse Problems at the Department of Industrial, Electronic and Mechanical Engineering. His research interests include artificial intelligence, non-linear optimization, and inverse problems applied complex systems, in particular power electronics, electromagnetic devices, and renewable energy.